Bmp2 and Notch cooperate to pattern the embryonic endocardium

Tania Papoutsi, Luis Luna-Zurita, Belen Prados, Stéphane Zaffran, Jose Luis de La Pompa

© 2018. Published by The Company of Biologists Ltd | Development (2018) 145, dev163378. doi:10.1242/dev.163378

RESEARCH ARTICLE

Bmp2 and Notch cooperate to pattern the embryonic endocardium

Tania Papoutsi[1,2], Luis Luna-Zurita[1,2,*], Belén Prados[1,2,*], Stéphane Zaffran[3] and José Luis de la Pompa[1,2,‡]

ABSTRACT

Signaling interactions between the myocardium and endocardium pattern embryonic cardiac regions, instructing their development to fulfill specific functions in the mature heart. We show that ectopic *Bmp2* expression in the mouse chamber myocardium changes the transcriptional signature of adjacent chamber endocardial cells into valve tissue, and enables them to undergo epithelial-mesenchyme transition. This induction is independent of valve myocardium specification and requires high levels of Notch1 activity. Biochemical experiments suggest that Bmp2-mediated Notch1 induction is achieved through transcriptional activation of the Notch ligand Jag1, and physical interaction of Smad1/5 with the intracellular domain of the Notch1 receptor. Thus, widespread myocardial Bmp2 and endocardial Notch signaling drive presumptive ventricular endocardium to differentiate into valve endocardium. Understanding the molecular basis of valve development is instrumental to designing therapeutic strategies for congenital heart valve defects.

KEY WORDS: Bmp2, Endocardium, Notch, Patterning, Signaling, Valve

INTRODUCTION

The early heart tube comprises primary myocardium (Moorman et al., 2003). As development proceeds, the myocardium becomes regionally specified into chamber and non-chamber tissue. The nascent chamber myocardium (ventricles and atria) is characterized by high proliferation rates (de Boer et al., 2012) and trabeculation (Sedmera et al., 2000). Non-chamber primary myocardium in the atrioventricular canal (AVC), outflow tract (OFT) and inner curvature is lined by extracellular matrix (ECM)-rich cushions and signals to the endocardium to activate the epithelial-mesenchyme transition (EMT) that gives rise to the mesenchyme of the valves and septa (Eisenberg and Markwald, 1995; Moorman et al., 2003). The primary myocardium in the AVC is characterized by expression of *Bmp2* from embryonic day (E) 8.5 onward (Sugi et al., 2004; Ma et al., 2005; Singh et al., 2005), *Tbx2* (Habets et al., 2002; Christoffels et al., 2004; Harrelson et al., 2004) and *Tbx3* (Hoogaars et al., 2004). Bmp2 directly activates *Tbx2* (Yamada et al., 2000; Ma et al., 2005).

Establishment of AVC myocardial identity and subsequent cushion formation are linked to EMT initiation and progression. *Bmp2*-deficient hearts show no AVC specification, fail to form endocardial cushions (Ma et al., 2005) and are unable to undergo EMT in explant cultures (Rivera-Feliciano and Tabin, 2006). Treatment of wild-type AVC explants with the Bmp antagonist Noggin represses EMT, as does the removal of the myocardial layer from untreated wild-type AVC explants. BMP2 is able to rescue the EMT in such cultures (Sugi et al., 2004) and to induce EMT in non-cushion-forming ventricular explants (Luna-Zurita et al., 2010), suggesting that Bmp2 is sufficient for EMT *ex vivo*.

Notch is a crucial signaling pathway during cardiac development, and its patterning role is highlighted by the specific expression of Notch elements in presumptive chamber and valve tissues (Del Monte et al., 2007). In early chamber endocardium, activation of the Notch1 receptor (N1ICD) is predominant in the endocardium at the base of the forming trabeculae, where Notch is essential for trabeculation (Grego-Bessa et al., 2007). In contrast, Notch is activated throughout the endocardium of presumptive valve territory (AVC and OFT); in these tissues, Notch promotes *Snail* transcription (Timmerman et al., 2004), and Bmp2-activated Smad leads to Snail activation and EMT (Luna-Zurita et al., 2010). Despite current knowledge of Bmp2-regulated AVC formation, EMT induction and its convergence with Notch, it remains unclear how Bmp2-mediated Smad affects endocardial Notch1 signaling.

Here, we examined the precise contribution of Bmp2 to AVC myocardial specification and its interplay with Notch to pattern the embryonic endocardium. We used a novel transgenic mouse model that enables conditional induction of *Bmp2* and unraveled the transcriptional events that follow *Bmp2* expression and lead to EMT induction, as well as the cooperation between Bmp and Notch in this process. EMT induction by Bmp2 is coordinated through the activation of a network of genes that regulate cell adhesion, intercellular communication, ECM deposition and proteasome-mediated protein degradation. EMT induction by Bmp2 does not take place in the absence of widespread Notch1 signaling. In fact, *Bmp2* ectopic expression in chamber myocardium causes activation of the Notch pathway throughout the ventricular endocardium, which then acquires the ability to undergo EMT. This occurs through transcriptional activation of the Notch ligand Jag1 by Bmp2-pSmad1/5, via direct binding of Smad1 to the *Jag1* promoter, as well as through the physical interaction of pSmad1/5 and N1ICD.

RESULTS

Gene profiling in *Bmp2^{GOF};Nkx2.5-Cre* hearts

We generated transgenic mice conditionally overexpressing Bmp2 (*Rosa26-Bmp2^{GOF}*; hereafter *Bmp2^{GOF}*; see Materials and Methods; Fig. S1A,B). *Bmp2^{GOF}* mice were crossed with the pan-cardiac driver line *Nkx2.5-Cre* (Fig. 1A; Fig. S1C) (Stanley et al., 2002). Only 53% (8/15) and 8% (1/13) of *Bmp2^{GOF};Nkx2.5-Cre* embryos examined survived to E10.5 and E11.5, respectively, with severe cardiac defects (Fig. S1D,E; Table S1A). At E9.5, *Bmp2* expanded from its normal AVC myocardium expression to the myocardium and endocardium in transgenic embryos (Fig. 1B; Fig. S2A). This led to phosphorylation of the effectors Smad1/5

[1]Intercellular Signaling in Cardiovascular Development and Disease Laboratory, Centro Nacional de Investigaciones Cardiovasculares Carlos III (CNIC), Melchor Fernández Almagro 3, 28029 Madrid, Spain. [2]Ciber de Enfermedades Cardiovasculares, Instituto de Salud Carlos III, Melchor Fernández Almagro 3, 28029 Madrid, Spain. [3]Aix Marseille Univ, INSERM, GMGF, UMR_S910, Faculté de Médecine, 27 Bd Jean Moulin, 13385 Marseille, France.
*These authors contributed equally to this work

‡Author for correspondence (jlpompa@cnic.es)

J.L.d.l.P., 0000-0001-6761-7265

Received 15 January 2018; Accepted 18 May 2018

Development (2018) 145, dev163378. doi:10.1242/dev.163378

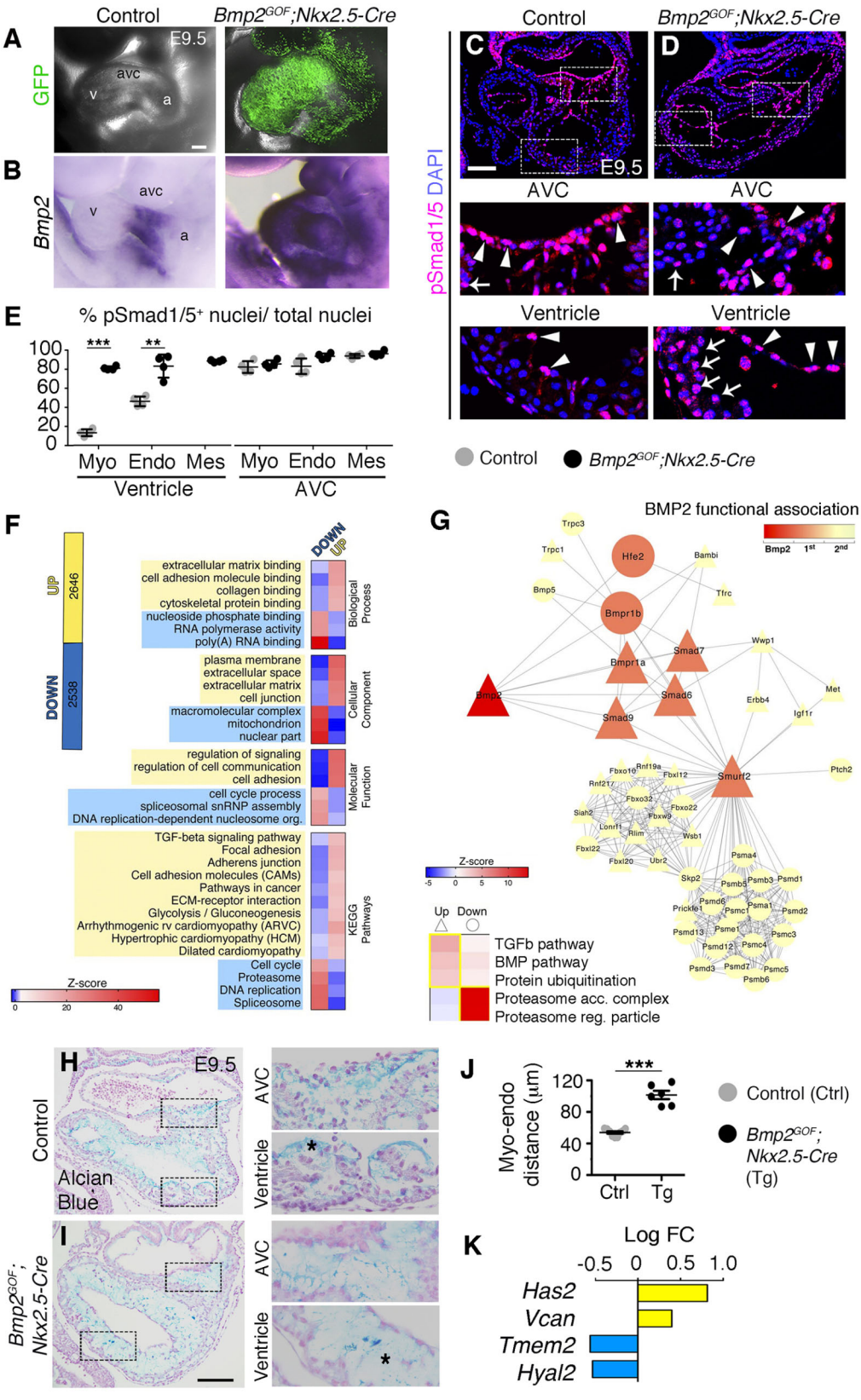

Fig. 1. Gene profiling of *Bmp2*^{GOF}*;Nkx2.5-Cre* hearts. (A) Efficient activation of GFP, associated with *Bmp2* transcription, in *Bmp2*^{GOF}*;Nkx2.5-Cre* hearts. (B) The restricted expression of *Bmp2* in the AVC myocardium of E9.5 control hearts is expanded throughout the heart in *Bmp2*^{GOF}*;Nkx2.5-Cre* embryos. (C,D) Phosphorylated Smad1/5 (pSmad1/5), showing expansion to ventricular myocardium in *Bmp2*^{GOF}*;Nkx2.5-Cre* hearts. (E) Quantification of myocardial, endocardial and mesenchymal pSmad1/5-positive (pSmad1/5^{+}) cells in AVC and ventricles. The data are % ratios of pSmad1/5^{+} cells to the total number of DAPI^{+} nuclei in each tissue. (F) Left. Chart showing the total number of DEGs identified by RNA-seq (P<0.005) in *Bmp2*^{GOF}*;Nkx2-5-Cre* hearts. Numbers in the yellow and blue sections indicate upregulated and downregulated genes, respectively. Right. Heat maps showing the GO and KEGG Pathway enrichment analyses in upregulated and downregulated genes. Red, high *z*-score; blue, low *z*-score. (G) Top. Bmp2-dependent interactome showing up to 2 degrees of physical or functional interaction of DEGs with Bmp2. Edges represent interactions between nodes (DEG). Triangles and circles represent upregulated and downregulated genes, respectively. Color represents the degree of neighborhood with Bmp2. Bottom. Heat map showing representative enriched GO terms associated with upregulated and downregulated genes with different degrees of interaction with Bmp2. Red, high *z*-score; blue, low *z*-score. (H,I) Alcian Blue staining showing excessive ECM accumulation in *Bmp2*^{GOF}*;Nkx2.5-Cre* ventricles. The limited space between ventricular myocardium and endocardium at E9.5 is increased in *Bmp2*^{GOF}*;Nkx2.5-Cre* hearts and filled with ECM (asterisks in insets). (J) Quantification of the distance (in µm) between myocardium and endocardium on histological sections of control and transgenic hearts. (K) Graph of the log-fold change (LogFC, RNA-seq) showing the upregulation of ECM-producing genes (yellow) and downregulation of ECM-degrading genes (blue). Scale bars: 100 µm. **P<0.01; ***P<0.001 (Student's *t*-test).

(Fig. 1C-E) and transcriptional activation of target genes (*Tgfb2* and *Smad6*) in both ventricular myocardium and endocardium of *Bmp2*^{GOF}*;Nkx2.5-Cre* hearts (Fig. S2B,C).

To study the effect of *Bmp2* overexpression on cardiac morphogenesis, we profiled E9.5 control and *Bmp2*^{GOF}*;Nkx2.5-Cre* hearts by RNA-seq. Transgenic hearts showed 5183 differentially expressed genes (DEGs), 2646 were upregulated and 2538 were downregulated (P<0.005) (Fig. 1F; Table S2, sheet one). The enrichment analysis of Gene Ontology (GO) terms revealed the over-representation of ECM, regulation of cell communication and

Development (2018) 145, dev163378. doi:10.1242/dev.163378

signaling, cell adhesion, cancer pathways and cardiomyopathy terms for the upregulated genes, and RNA regulation, proteasome, cell cycle and proliferation terms for the downregulated genes (Fig. 1F; Table S2, sheets two and three).

To identify the DEGs with the closest hierarchical relation with respect to Bmp2, we generated a Bmp2-dependent network by integrating the 2000 DEGs with the lowest *P*-value with the STRING database (Szklarczyk et al., 2015). We isolated the DEGs with up to two degrees of neighborhood with Bmp2 and predicted a network of 57 nodes or genes (Fig. 1G). Among the direct interactors of Bmp2 (Fig. 1G, orange nodes), the Bmp receptor *Bmpr1a*, Smad effectors and *Smurf2*, a ubiquitin ligase that negatively regulates Smad proteins (Zhang et al., 2001), appeared upregulated, confirming the functional overactivation of Bmp2 (Fig. 1G). Interestingly, Smurf2 was connected to the majority of the second-degree interactors (Fig. 1G, yellow nodes), which were mostly downregulated and involved in proteasome regulation (Fig. 1G, bottom left). We confirmed the increased expression of both *Smurf1* and *Smurf2* in ventricular endocardium of transgenic hearts (Fig. S2D-F, black arrowheads).

The over-representation of ECM-related terms in the RNA-seq and the known role of Bmp2 in ECM regulation (Ma et al., 2005; Rivera-Feliciano and Tabin, 2006) prompted us to look into ECM deposition. Alcian Blue staining showed ECM accumulation (Fig. 1H,I and insets) and histological measurements revealed a significantly increased myocardium–endocardium distance in *Bmp2^{GOF};Nkx2.5-Cre* ventricles (Fig. 1J). Increased expression of ECM-producing genes (*Has2* and *Vcan*) and downregulation of ECM-degrading genes (*Tmem2* and *Hyal2*) could explain the observed phenotype (Fig. 1K).

To identify the most affected processes within the high number of DEGs, we focused on the upregulated genes with the highest number of direct connections with other DEGs. GO analysis of this subgroup showed enrichment in cancer, cell adhesion and dilated cardiomyopathy terms (Fig. S2G; Table S2, sheet six). Cancer and adhesion terms are commonly related to EMT, cell migration and motility. We then compared our E9.5 *Bmp2* GOF heart RNA-seq data with a E11.5 *Bmp4* GOF mandibular tissue microarray (Bonilla-Claudio et al., 2012). We found 36 common upregulated genes, including known Bmp signaling targets, such as *Id1*, *Msx2* and *Tbx20*. We also observed 95 genes that changed direction in the two data sets, which suggests tissue-specific transcriptional network regulation (Table S3). To obtain a more comprehensive comparison of Bmp regulation during early stages of development, we compared our current E9.5 Bmp2 GOF heart RNA-seq with an E14.5 Bmp2 GOF heart RNA-seq (Prados et al., 2018). This comparison (Table S4) highlighted several common upregulated and downregulated genes related to muscle, heart muscle and/or ventricular development (shown in dark red in Fig. S3), cardiac valve development (yellow in Fig. S3) and Bmp signaling (blue in Fig. S3).

Induction of ectopic EMT in *Bmp2^{GOF};Nkx2.5-Cre* hearts

We set out to characterize the effect of excessive myocardial *Bmp2* on EMT *in vivo*. Hematoxylin & Eosin (H&E) staining of E9.5 *Bmp2^{GOF};Nkx2.5-Cre* hearts revealed an expanded AVC (Fig. 2A, B, double arrows; Fig. 2C, measurements) filled with mesenchymal cells (Fig. 2A,B insets, arrowheads). Mesenchymal cells in transgenic embryos were also found throughout the ventricles (Fig. 2B inset, arrowhead), adjacent to the endocardium, which was localized in the center of the lumen instead of closely lining the myocardium (Fig. S4A-F).

The RNA-seq analysis of *Bmp2^{GOF};Nkx2.5-Cre* hearts showed increased expression of cardiac EMT-related genes, such as *Snail2/3*, *Sox9*, *Vim* and *Twist1* (Fig. 2D). Immunostaining or *in situ* hybridization in sections confirmed the expansion of *Sox9*, *Snail1* and *Twist1* to the ventricular endocardium in transgenic hearts (Fig. 2E-H; Fig. S4G,H). Thus, histological and expression data suggest that the transgenic ventricular endocardium molecularly resembles the endocardium of the AVC and, thus, that it acquired the ability to undergo EMT. To test this possibility, we used *ex vivo* explant cultures on collagen gels (Runyan and Markwald, 1983). Control and transgenic AVC endocardial cells were able to migrate and invade the gel (measured by their three-dimensional transformation index, 3D TI; Fig. 2I,J,M; Movies 1,2). Explanted control ventricles did not undergo EMT, but instead formed a continuous endothelial monolayer (Fig. 2K) (Luna-Zurita et al., 2010). By contrast, *Bmp2^{GOF};Nkx2.5-Cre* ventricular endocardial cells transformed and invaded the gel, behaving like AVC endocardium (Fig. 2L,M; Movies 3,4). Transgenic ventricular endocardial cells migrated further and invaded deeper than their control counterparts, reaching similar levels to AVC endocardial cells (Fig. S4I,J). Interestingly, transgenic ventricular endocardial also lacked the expression of *Irx5* (Fig. S4K,L), a known marker of ventricular endocardium (Christoffels et al., 2000; Bruneau et al., 2001), indicating the loss of ventricular endocardium identity.

The myocardium of transgenic ventricles was thinner and had small trabeculae (Fig. S5A), but a relatively normal gene expression profile, compared with control ventricles: it expressed chamber differentiation markers (*Irx4*, *Myl2*, *Bmp10* and *Nppa*) and lacked AVC markers (*Tbx2* and *Tbx3*) (Fig. S5B-K). Myocardial cell proliferation, assessed by BrdU incorporation, was reduced in *Bmp2^{GOF};Nkx2.5-Cre* hearts, accounting for the thinner myocardium (Fig. S5L,M). These results were confirmed with earlier activation of *Bmp2* throughout the mesoderm with the *Mesp1-Cre* driver (Fig. S6; Table S1B).

Increased Notch1 activity in *Bmp2^{GOF};Nkx2.5-Cre* hearts

Notch1 activity is indispensable for EMT (Timmerman et al., 2004; Luna-Zurita et al., 2010). We next examined whether the expansion of EMT in *Bmp2^{GOF};Nkx2.5-Cre* hearts was accompanied by expanded Notch1 activity. At E9.5, Notch1 pathway activation, detected by nuclear staining of N1ICD, occurred throughout the AVC endocardium (Fig. 3A, arrowhead) but was restricted to a subset of ventricular endocardial cells (Fig. 3A inset, arrowheads). N1ICD staining in *Bmp2^{GOF};Nkx2.5-Cre* hearts was observed throughout the endocardium (Fig. 3B and inset), leading to a twofold increase in N1ICD protein levels (Fig. 3C,D). Our RNA-seq data showed increased expression of various components of the Notch pathway (Fig. 3E). The upregulation of Notch ligands by *Bmp2* overexpression could explain the observed increase in Notch activity. Thus, we assessed the expression patterns of *Dll4* and *Jag1*, the most relevant ligands at E9.5 (D'Amato et al., 2016; MacGrogan et al., 2016). *Dll4*, normally restricted to a subset of ventricular endocardial cells at this stage, was expanded throughout the endocardium in transgenic hearts (Fig. 3F, white arrowheads). *Jag1*, normally restricted to the myocardium in the ventricles, was found ectopically expressed in the ventricular endocardium of *Bmp2^{GOF};Nkx2.5-Cre* hearts (Fig. 3G, white arrowheads). In contrast to *Dll4*, *Jag1* did not appear upregulated in the RNA-seq, likely because of its predominant myocardial expression in normal E9.5 hearts, which, together with the myocardial thinning in transgenic hearts (Fig. 3G black arrowheads and quantification in Fig. S5M), masked any difference in gene expression levels. *In situ* hybridization of the Notch targets *Hey1*, *Hey2* and *Heyl* confirmed the expanded Notch activity in the ventricular endocardium of transgenic hearts (Fig. 3H-J).

Development (2018) 145, dev163378. doi:10.1242/dev.163378

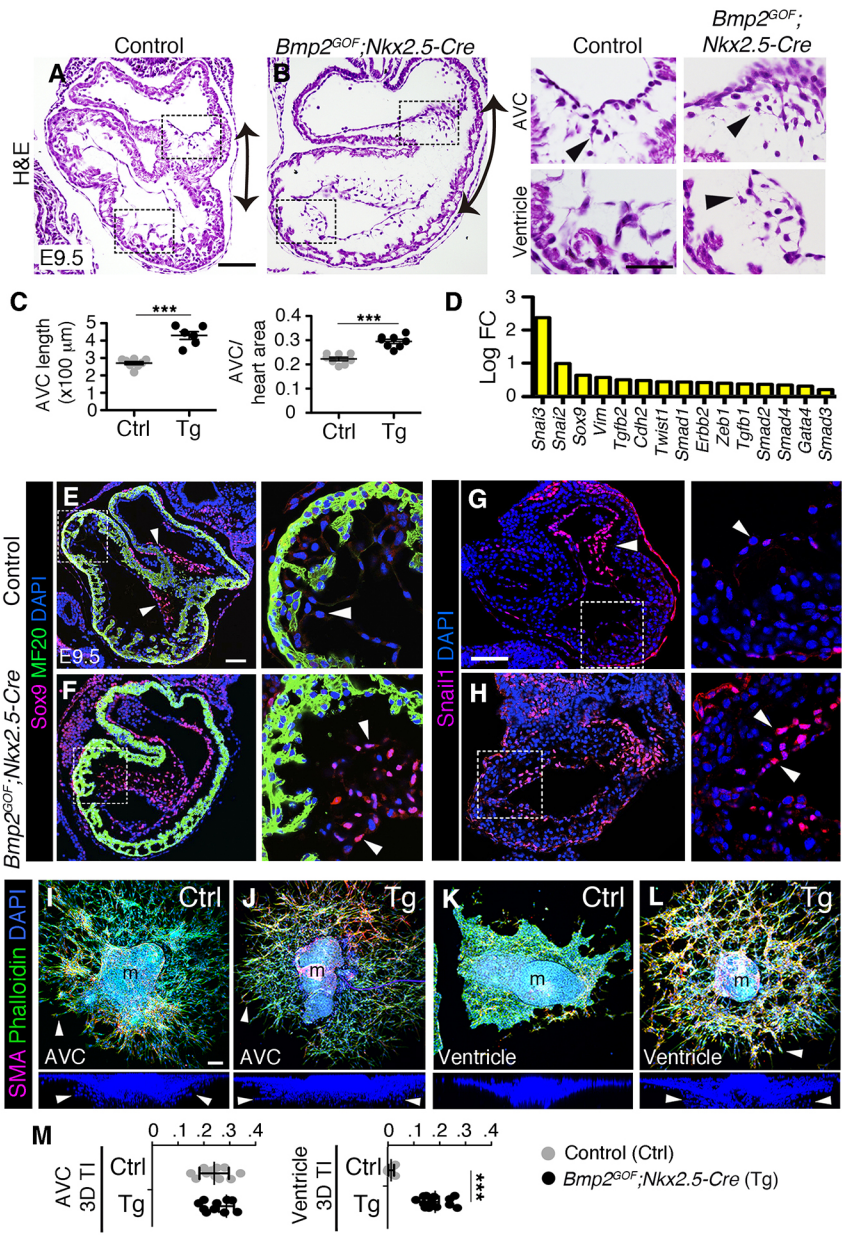

Fig. 2. Ectopic *in vivo* EMT induction in *Bmp2^{GOF};Nkx2.5-Cre* hearts. (A,B) H&E staining of E9.5 *Bmp2^{GOF};Nkx2.5-Cre* hearts, revealing mesenchymal cells in the ventricle, reminiscent of the population normally restricted to the AVC (black arrowheads). The double arrows indicate expansion of the AVC territory. (C) AVC measurements of histological sections: the length of the AVC (µm) and the area occupied by the AVC as a proportion of the total heart area (ratio) in control and *Bmp2^{GOF};Nkx2.5-Cre* hearts. (D) Graph of the log-fold change (LogFC, RNA-seq) showing the upregulation of cardiac EMT-inducing genes. (E,F) Ventricular expansion of the EMT marker Sox9 (magenta), in *Bmp2^{GOF};Nkx2.5-Cre* hearts (arrowheads). MF20 (green) was used as a myocardial marker. (G,H) Expansion of Snail1 (magenta) in *Bmp2^{GOF};Nkx2.5-Cre* embryos to ventricular endocardium and the ectopically produced mesenchyme (arrowheads). (I-L) AVC and ventricular explants cultured on collagen gels. Explants were immunostained with a mesenchymal marker (α-smooth muscle actin, SMA, magenta) and an actin cytoskeletal marker (phalloidin, green). Maximal confocal projections of the *x-y* and *x-z* axes are shown. (I,J) Control and *Bmp2^{GOF};Nkx2.5-Cre* AVC explants showing mesenchymal 3D invasion. (K) Endocardial cells of control ventricular explants form a monolayer on the gel surface and do not undergo EMT. (L) Endocardial cells of *Bmp2^{GOF};Nkx2.5-Cre* ventricles undergo EMT, behaving like AVC endocardial cells. In the *x-z* axis images, only DAPI is shown for clarity. Arrowheads point to invading cells. (M) 3D TI quantification of control and *Bmp2^{GOF};Nkx2.5-Cre* AVC and ventricles; 3D TI was calculated as the ratio of gel-invading cells to total cell number. Eight to ten explants were counted per condition. See also Movies 1-4. m, myocardium. Scale bars: 100 µm. ***P<0.001 (Student's t-test).

To establish whether Bmp2-dependent Notch activation is a prerequisite for EMT induction, we performed explant cultures, as described before, and blocked Notch signaling with the γ-secretase inhibitor RO4929097 (RO). Cell invasiveness in control and transgenic AVC explants (Fig. 3K,N) and in transgenic ventricular explants (Fig. 3L,O) was severely suppressed in the absence of Notch activity (Fig. 3M,P; Movies 5,6). Thus, Bmp2-induced ectopic EMT is mediated by Notch1.

To establish the source of Bmp2 responsible for the observed endocardial phenotype, we activated *Bmp2* using myocardium- or endocardium-specific drivers (Fig. S7). *Bmp2$^{GOF/+}$;cTnT-Cre* embryos (myocardial *Bmp2*) recapitulated the *Bmp2^{GOF};Nkx2.5-Cre* phenotype (ECM accumulation, expanded N1ICD and EMT; Fig. S8B,E,H,K,N,Q; Table S1C), whereas *Bmp2$^{GOF/+}$;Tie2-Cre* and *Bmp2$^{GOF/GOF}$;Tie2-Cre* embryos (endothelial *Bmp2*) appeared normal at E9.5 (Fig. S8C,F,I,L,O,R; Table S1D). Therefore, we concluded that induction of Notch1 and ectopic EMT *in vivo* is driven by myocardial Bmp2.

Bmp-activated Smad1 binds to the *Jag1* promoter

The ectopic endocardial expression of *Jag1* in *Bmp2^{GOF};Nkx2.5-Cre* ventricles (Fig. 3G) prompted us to study how this activation occurs. To test for a possible direct activation of *Jag1* transcription by Bmp2-pSmad1, we performed chromatin immunoprecipitation (ChIP) experiments with an anti-Smad1 antibody on mouse embryonic ventricular endocardial cells (MEVECs) (D'Amato et al., 2016), treated or not with recombinant human BMP2. We assessed the binding of Smad1 to two Smad1/5-binding regions in the *Jag1* locus (Morikawa et al., 2011): one in the promoter region (approximately 520 bp upstream of the transcriptional start site, TSS) and one within the second intron (Fig. S9). Quantitative PCR (qPCR) analysis of the immunoprecipitated DNA with primers flanking the Smad1-binding regions showed a significant enrichment of the promoter region after BMP2 stimulation in contrast to untreated cells (Fig. 4A). This enrichment was only observed after BMP2 treatment. We also observed a significant increase in the expression levels of *Jag1* in this system (Fig. 4B),

Development (2018) 145, dev163378. doi:10.1242/dev.163378

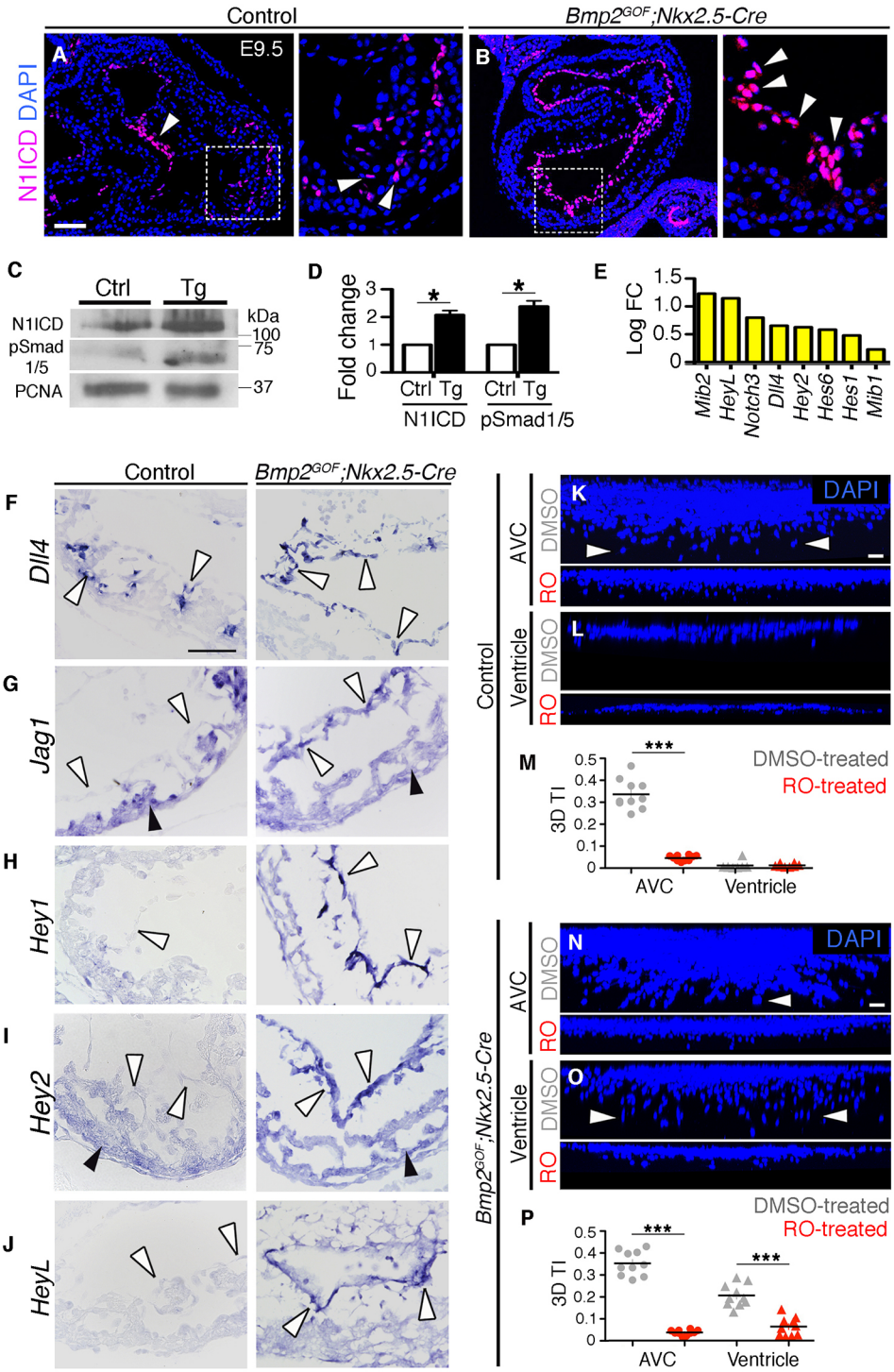

Fig. 3. Increased Notch1 activity in *Bmp2^{GOF};Nkx2.5-Cre* hearts is a prerequisite for ectopic EMT induction. (A) N1ICD staining (magenta), showing Notch1 pathway activity, is detected throughout the AVC endocardium (arrowhead) and in some endocardial cells in the ventricle at E9.5 (arrowheads in inset). (B) N1ICD staining is expanded to all endocardial cells in transgenic hearts (arrowheads). (C) Western blot of E9.5 control (ctrl) and *Bmp2^{GOF};Nkx2.5-Cre* (tg) hearts with anti-N1ICD, anti-pSmad1/5 and anti-PCNA (nuclear marker) antibodies. (D) Graph with the normalized ratios of N1ICD and pSmad1/5 to PCNA. (E) Graph of the log-fold change (LogFC, RNA-seq) showing the upregulation of Notch-related genes. (F-J) High-magnification *in situ* hybridization images of control and *Bmp2^{GOF};Nkx2.5-Cre* ventricles. (F) *Dll4*, normally found in some ventricular endocardial cells located at the base of the forming trabeculae at E9.5, is expressed throughout the ventricular endocardium in *Bmp2^{GOF};Nkx2.5-Cre* hearts (arrowheads). (G) *Jag1* is normally expressed in ventricular myocardium (black arrowheads) and not in ventricular myocardium (white arrowheads) at E9.5. In transgenic ventricles, *Jag1* is ectopically expressed in the endocardium (arrowheads). (H) The endocardial expression of *Hey1*, normally restricted to the AVC and almost undetectable in control ventricular endocardium, is expanded into the chambers in transgenic embryos (white arrowheads). (I) *Hey2* is normally expressed in ventricular myocardium (black arrowheads) and is almost undetectable in ventricular endocardium (white arrowheads). In transgenic ventricles, *Hey2* is expanded into chamber endocardium (white arrowheads). (J) A similar expansion was observed for *Heyl* (white arrowheads). (K,L) Effect of RO on the invasive ability of AVC and ventricular explants. DMSO was used as the vehicle. Only endocardial and endocardial-derived mesenchymal cells are DAPI stained in these maximal confocal *z*-projections. Quantification of the effect of RO on the 3D TI [graphs (M,P)] revealed significantly reduced invasion. Circles represent AVC and triangles ventricular explants. Eight to ten explants were counted per condition. See also Movies 5 and 6. Scale bars: 100 µm (A,K,L,N,O); 50 µm (F-J). *P<0.05, ***P<0.001 (Student's *t*-test).

likely mediated by Smad1 binding to its promoter. Consistent with these data, activation of the Bmp pathway by transfection of the constitutively active Bmp receptor Alk3 (caAlk3) in endothelial cells, resulted in significant induction of a luciferase reporter containing the mouse *Jag1* promoter (Fig. 4C) and only minimal induction of the *Jag1* intronic region (Fig. 4D).

Bmp-pSmad1/5 and Notch cooperation

To understand how Bmp2 interacts with Notch in more depth, we used MEVEC co-cultured with OP9 cells expressing either GFP (control), or the Notch ligands Jag1 or Dll4 (Fig. S10A). OP9-Jag1 cells induced Notch activity, shown by *Hey1*, *Hey2* and *Heyl* upregulation, in MEVEC (Fig. 5A, gray versus white bars). Addition of BMP2 in these co-cultures activated Bmp targets (Fig. S10B) and further increased the expression of *Hey1* and *Heyl* (Fig. 5A, black/gray versus gray bars) and led to threefold increased N1ICD protein levels, as shown by western blot analysis (Fig. 5C, input and quantification). These findings suggest that Bmp2 enhances Notch pathway activity *in vitro*. Treatment of the OP9-GFP/MEVEC co-cultures with BMP2 also led to a significant increase in *Hey1* and *Heyl* expression (Fig. 5A, black versus white bars), which suggests that Bmp2 activates the Notch pathway even

Development (2018) 145, dev163378. doi:10.1242/dev.163378

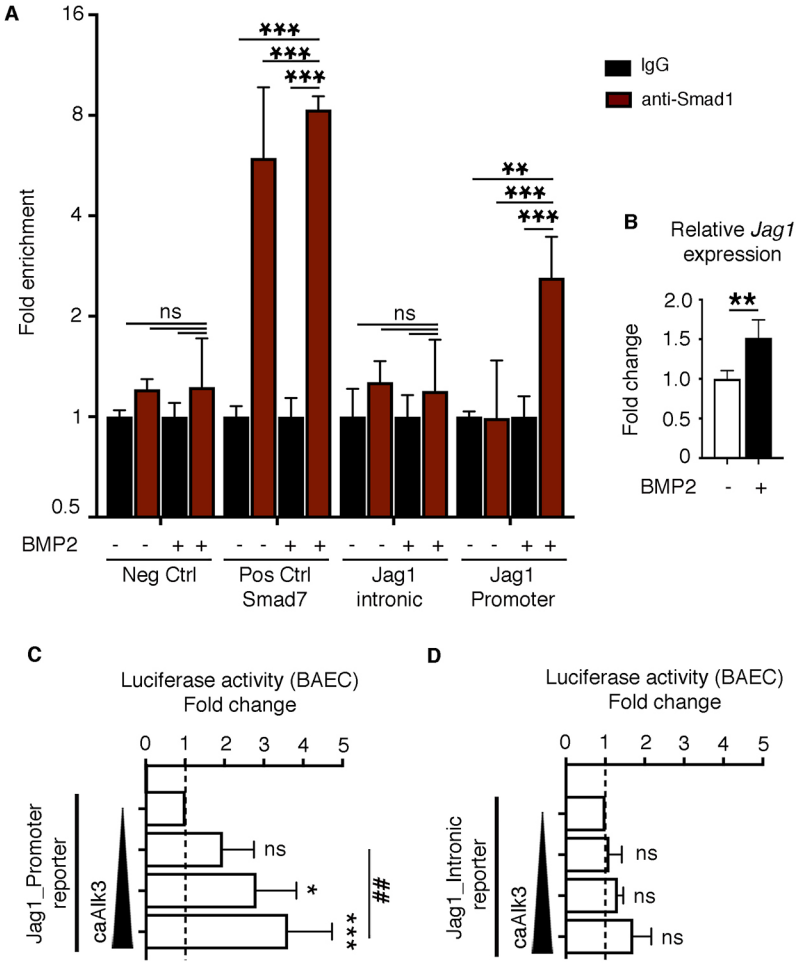

Fig. 4. Bmp-activated Smad1 binds to the *Jag1* promoter. (A) Smad1 ChIP-quantitative PCR on MEVECs. Control and BMP2-stimulated MEVECs were subjected to ChIP assays with anti-Smad1 or control IgG. qPCR on immunoprecipitated chromatin from BMP2-stimulated MEVECs shows enrichment of Smad1 in the promoter but not in the intronic region of the Jag1 locus. Primers against a known Smad1-dependent regulatory region in the promoter of Smad7 served as positive control. Primers against a gene-poor region served as a negative control. Data are represented as mean-fold enrichment±s.d. of at least three independent experiments. (B) qRT-PCR data showing increased *Jag1* expression after treatment of MEVECs with recombinant BMP2. (C,D) Luciferase assays in BAECs transfected with a reporter plasmid (pGL3) containing either the promoter or the intronic region of mouse *Jag1*. Endogenous reporter activation (dashed line) was recorded in cells transfected with only empty vectors and the *Renilla* internal control. Transfection with increasing amounts of caAlk3 (25, 50 and 75 ng) activates the promoter reporter in a dose-dependent manner and only minimally stimulates the intronic reporter. **P*<0.05; ***P*<0.01; ##*P*<0.01; ****P*<0.001 (one-way ANOVA, multiple comparisons).

in the absence of strong Notch signals. Bmp2-mediated activation of *Jag1* expression, likely via direct binding of Smad1 to its promoter, could induce the Notch pathway in adjacent cells. Indeed, we observed the induction of *Jag1* expression in BMP2-treated OP9-GFP/MEVEC co-cultures (Fig. 5B, black versus white bars). By contrast, *Jag1* was not upregulated after Dll4-Notch induction (Fig. S10C; Fig. 5B, green bar) and no synergistic effect was observed after activation of both pathways (Fig. 5B, green/black bar). These findings suggest that Bmp2-mediated induction of *Jag1* is independent of Notch, whereas activation of *Dll4* by Bmp2 can only take place in the presence of Notch signals.

To explain the synergistic effect of Bmp and Notch signaling on gene expression, we tested for a potential physical interaction between N1ICD and pSmad1/5. After confirming the activation of N1ICD upon BMP2 stimulation (Fig. 5C), we immunoprecipitated (IP) OP9-Jag1/MEVEC (±BMP2) lysates with anti-Notch1 or anti-Smad1, and blotted with both antibodies. In BMP2-treated co-cultures, we detected pSmad1/5 in the Notch1-IP and N1ICD in the Smad1-IP (Fig. 5D,E), suggesting that the two proteins physically interact. We confirmed these results in BAEC, where we were able to co-IP pSmad1/5 and Myc-tagged N1ICD (Myc-N1ICDΔ^{OP}) (Milner et al., 1996) (running at 70 kDa; Fig. S11A,B). We also confirmed the ability of Bmp2 to induce Notch activity by performing luciferase assays on endothelial cells (BAEC). A Notch reporter containing ten consecutive CBF1/RBPJ-binding sites (McKenzie et al., 2005) was stimulated by caAlk3 in the absence and presence of N1ICD (Fig. 5F; Fig. S11C,D).

Given the low levels of the two proteins and the small size of the heart at E9.5, we were not able to perform this IP *in vivo*. However, we believe that MEVECs, isolated from E10.5 ventricles and stimulated *in trans* by OP9 cells (for Notch activation) or with recombinant BMP2 (for Bmp activation), are a physiologically relevant system. *In vivo* at E9.5, pSmad1/5 and N1ICD colocalized only minimally in ventricular endocardial cells (Fig. S12A, inset, white arrowhead). In transgenic hearts, the colocalization was more extensive (Fig. S12B, inset, white arrowheads), supporting a possible physical interaction between the proteins.

Together, our results show that Bmp2-pSmad1 is able to activate the transcription of the Notch ligand Jag1 by direct binding to its promoter, thus inducing Notch activity and target gene transcription. In cells where both pathways are active, Notch target gene expression is enhanced through the activation of Notch ligands and the interaction of the effectors pSmad1/5 and N1ICD.

DISCUSSION

Bmp2 is an essential signal that specifies the primitive AVC primary myocardium of the embryonic heart (Ma et al., 2005; Rivera-Feliciano and Tabin, 2006) versus the differentiated myocardium of the chambers. Myocardial Bmp2 expression drives a gene expression program that leads to formation of the valve primordium, in concert with endocardial-derived signals, such as Notch. Indeed, the differential distribution of N1ICD patterns the early valve and chamber endocardium, with widespread and relatively uniform expression in valve endocardium but restricted to the base of

Development (2018) 145, dev163378. doi:10.1242/dev.163378

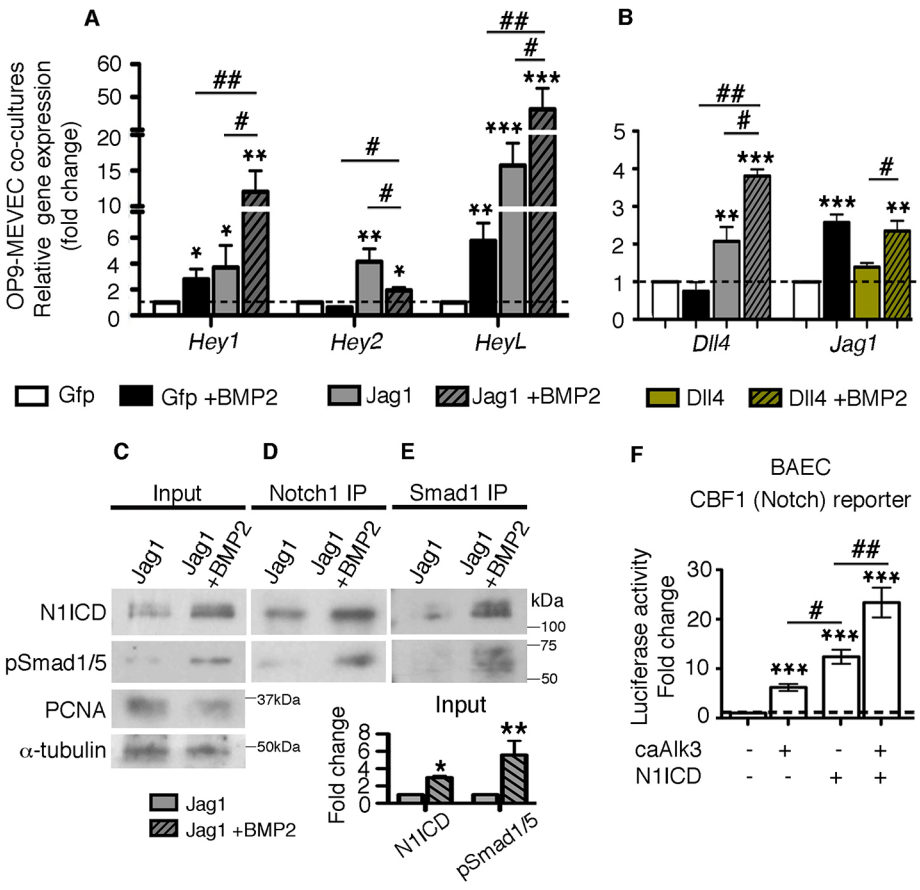

Fig. 5. Bmp-pSmad1/5 and Notch cooperation. (A) Notch target gene expression analysis in MEVECs co-cultured with OP9 cells expressing GFP (control) or Jag1 in the presence or absence of human recombinant BMP2. (B) Notch ligand expression analysis in MEVECs co-cultured with OP9 cells expressing GFP (control), Jag1 or Dll4 in the presence or absence of human recombinant BMP2. (C) Input. Western blot of MEVECs co-cultured with OP9 cells expressing Jag1 in the presence or absence of BMP2 with anti-Notch1, anti-pSmad1/5, anti-PCNA (nuclear loading control) and anti-α-tubulin antibodies. Graph. Quantification of the input western blot, showing the normalized ratios of N1ICD and pSmad1/5 to PCNA. (D) Notch1 IP. Western blot of Notch1 immunoprecipitates (IP) with anti-Notch1 and anti-pSmad1/5 antibodies. (E) Smad1 IP. Western blot of Smad1 IP with anti-Notch1 and anti-pSmad1/5 antibodies. (F) Luciferase assay in BAECs transfected with the CBF1-Luc (Notch) reporter. Endogenous reporter activation (dashed line) was recorded in cells transfected with only empty vectors and the *Renilla* internal control. Transfection with 50 ng caAlk3-expressing plasmid increases reporter activity 5-fold and transfection of 10 ng N1ICD-expressing plasmid by 13-fold. Simultaneous transfection of both plasmids further increases reporter activity (22-fold compared with endogenous levels and 1.7-fold compared with N1ICD alone). **P*<0.05; ***P*<0.01; ****P*<0.001 (Student's *t*-test, compared with the GFP condition or the endogenous reporter activity); #*P*<0.05; ##*P*<0.01 (Student's *t*-test, compared with individual controls).

developing trabeculae in the ventricles (Timmerman et al., 2004; Del Monte et al., 2007; Grego-Bessa et al., 2007; MacGrogan et al., 2016). The combined activities of myocardial Bmp2 and endocardial Notch1 pattern the AVC and regulate the process of EMT (Luna-Zurita et al., 2010), which is crucial for valve development. Our study focused on the analysis of a novel mouse model conditionally overexpressing *Bmp2*, to identify global Bmp2-induced transcriptional changes associated with the regulation of valve EMT, and to shed light on the cooperation between Bmp2 and Notch1 signals.

Our results revealed the ability of pan-myocardial Bmp2 to specify ventricular endocardium as valve tissue, and to induce ectopic EMT in the ventricles. This is achieved via the transcriptional activation of several EMT drivers, including Snail1, Twist1 and Sox9, the expression of which is upregulated and expanded to the endocardium of the ventricles in transgenic embryos. Genes related to ECM regulation, cell adhesion, cell migration and intercellular signaling were also upregulated. Likewise, both *Smurf1* and *Smurf2*, involved in the dissolution of tight junctions and in TGFβ-induced EMT (Ozdamar et al., 2005; Townsend et al., 2008; Chandhoke et al., 2016), were upregulated in Bmp2-overexpressing hearts. Thus, Smurf-mediated proteasome regulation of proteins (cytoskeletal, epithelial and junctional) might have a crucial role in the initiation of EMT under the control of Bmp2. The loss of expression of the chamber endocardium marker *Irx5*, together with the gain of the EMT drivers and effectors described above, suggest the conversion in transgenic embryos of ventricular endocardium into valve tissue.

Endocardial Notch1 pathway activation is a crucial step in EMT induction by Bmp2. Notch1 activity is sufficient to activate a pro-mesenchymal gene program through *Snai1l2* induction, but completion of EMT and invasion of the cardiac jelly is achieved through Bmp2, which promotes Snail1 protein stabilization (Luna-Zurita et al., 2010). *Bmp2*-overexpressing hearts showed complete Notch1-dependent EMT in *ex vivo* ventricular cultures and *in vivo* within the ventricle. Transgenic ventricular endocardial cells migrated more efficiently than their control counterparts, but did not exceed the migration and invasion levels of AVC endocardial cells, either control or transgenic.

Interestingly, ectopic expression of Bmp2 in chamber myocardium of *Bmp2^{GOF};Nkx2.5-Cre* embryos was unable to activate a full AVC myocardial program in the chambers, although this was not necessary for endocardial EMT to occur. Overexpression of *Tbx2* (or *Tbx3*) in the heart tube represses ventricular myocardium genes (Christoffels et al., 2004; Hoogaars et al., 2007; Shirai et al., 2009; Singh et al., 2012). Bmp2 is essential for the activation of *Tbx2* through pSmad1/5 transcriptional induction, which is in turn regulated by Tbx20 (Harrelson et al., 2004; Shirai et al., 2009; Singh and Kispert, 2010). High Tbx20 levels induced by Bmp2 could prevent the excessive pSmad1/5 from transcriptionally activating *Tbx2*, allowing for chamber myocardium genes to be normally expressed.

Our initial observation that ectopic *Bmp2* profoundly affected Notch1 activity *in vivo* prompted us to examine how this activation occurs. We showed that Notch1 activity was responsive to Bmp2 signals in endocardial and endothelial cells *in vitro*: N1ICD was increased, *Hey* genes were upregulated, and a Notch reporter was stimulated after Bmp pathway activation. Here, we propose that this activation occurs in two distinct ways, depending predominantly on the endogenous Notch levels: protein interaction and transcriptional induction.

We showed in two different cellular models that pSmad1/5 and N1ICD physically interact. Smad1 and Smad3 can bind N1ICD,

Development (2018) 145, dev163378. doi:10.1242/dev.163378

recruit p300 and stabilize the Notch transcriptional complex, along with P/CAF, in specific promoter regions, thus reinforcing pathway activity in myoblasts, endothelial and neuroepithelial cells (Blokzijl et al., 2003; Takizawa et al., 2003; Itoh et al., 2004; Moya et al., 2012). In epithelial cells, the common Bmp mediator Smad4 is also important for the synergistic activation of a Notch reporter (Itoh et al., 2004). Binding of pSmad1/5 to N1ICD in endocardial cells could act in a similar manner to stabilize the Notch complex. However, this protein interaction likely takes place only in the presence of high pSmad1/5 and N1ICD levels within the same cell. In N1ICD-negative or N1ICD-low cells, pSmad1/5 might trigger Notch pathway induction via the transcriptional activation of its ligands.

We also showed that Bmp2 alone transcriptionally activates the Notch ligand *Jag1* in endocardial cells, by direct binding of Smad1 to its promoter, as has been shown in other systems (Morikawa et al., 2011). In turn, Jag1 binds to Notch receptors in adjacent cells, activating the pathway and inducing *Hey* gene transcription. Once the Notch pathway is active, BMP2 further enhances the expression of *Dll4*, *Hey1* and *Heyl*.

We suggest that, in E9.5 wild-type hearts, the specification of AVC endocardium results from the interplay between myocardial Bmp2 and endocardial Notch1 signaling (Fig. 6). pSmad1/5 transcriptionally activates Notch ligands in AVC endocardium, leading to widespread Notch1 activity in this tissue. This allows for physical interaction between the abundant pSmad1/5 and N1ICD, which further enhances Notch1 activity. The combined effect of both pathways triggered the transcription in the AVC of genes inducing EMT (Fig. 6A,C). In the ventricles, low Bmp signaling and restricted endocardial Notch activity prevented the physical interaction of the

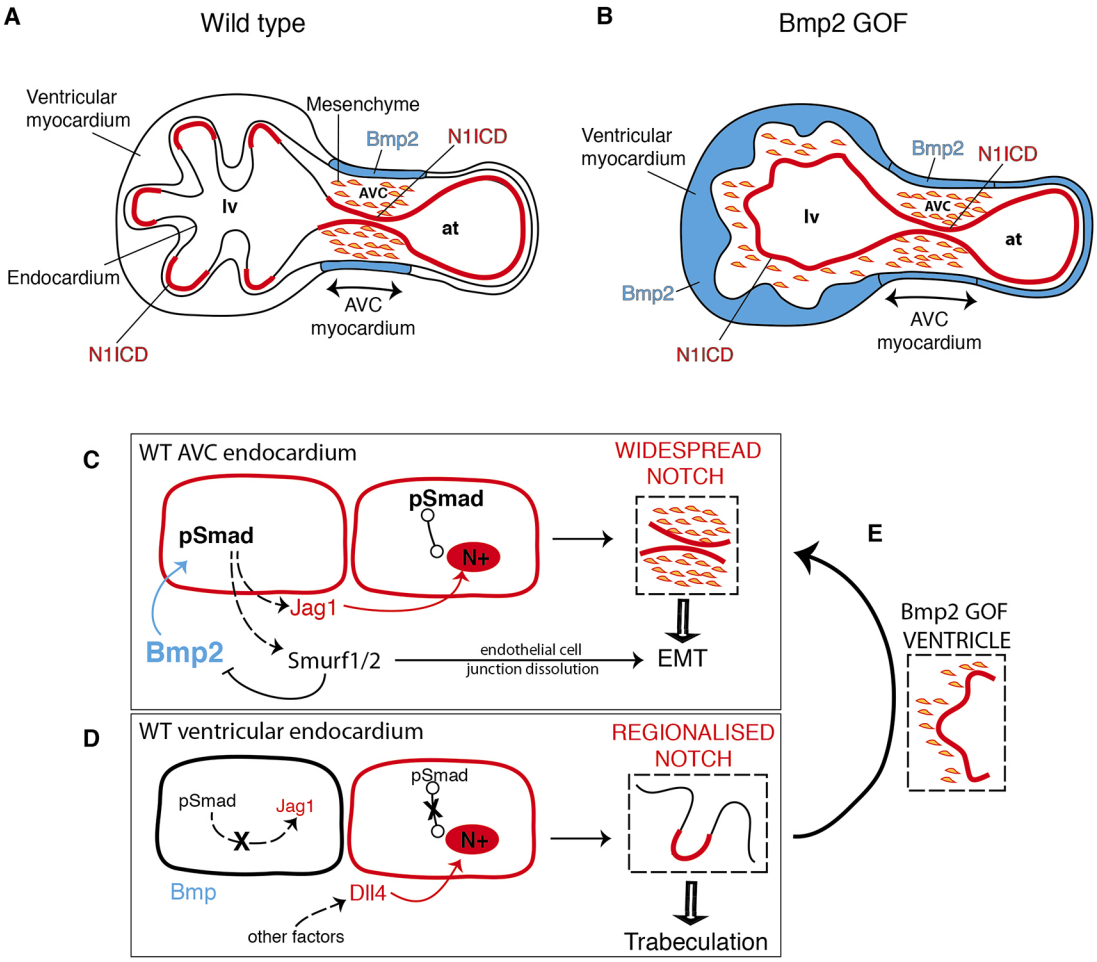

Fig. 6. Proposed model of Bmp2 and Notch1 interplay. (A) E9.5 wild-type heart. *Bmp2* expression (blue) is restricted to the AVC myocardium. The AVC-restricted pattern induces Notch1 activity and EMT in the underlying endocardium. Endocardial-derived mesenchymal cells (orange) are found in the AVC. N1ICD expression is high and uniform in AVC endocardium and in the atrium (red), whereas, in ventricular endocardium, Notch1 is active only at the base of the forming trabeculae. (B) E9.5 *Bmp2^{GOF};Nkx2.5-Cre* (also *Bmp2^{GOF};cTnT-Cre* and *Bmp2^{GOF};Mesp1-Cre*) heart. *Bmp2* expression throughout the myocardium (blue) results in widespread endocardial Notch1 activity (red), patterning the ventricular endocardium as AVC endocardium and leading to ectopic EMT in the ventricle (orange mesenchymal cells). Myocardial identity is unaffected. (C) In AVC endocardium, Bmp2-induced pSmad1/5 transcriptionally activates *Jag1* by direct binding to its promoter, which in turn activates the Notch pathway in adjacent cells expressing Notch receptors (N+; N1ICD-positive cells). Binding of the effectors pSmad1/5 and N1ICD (white circles) reinforces the Notch-mediated transcription of target genes. High N1ICD further propagates Notch pathway activation throughout the AVC endocardium. Cooperation between the two pathways (Bmp and Notch) induces the transcription of genes triggering EMT induction and progression. (D) In the ventricle, low Bmp signaling is not sufficient to activate Jag1. Induction of *Dll4* by other factors locally activates the Notch pathway. Low levels of pSmad1/5 do not allow for physical interaction with N1ICD and, thus, N1ICD activation remains regionalized. Therefore, the endocardium shows features of chamber tissue and trabeculation occurs. (E) Ectopic myocardial expression of *Bmp2* (in *Bmp2^{GOF};Nkx2.5-Cre,Bmp2^{GOF};cTnT-Cre* hearts) converts ventricular endocardium to AVC endocardium via expansion of Notch signaling. White circles indicate physical interactions. Red or black cell membranes represent the expression or absence of Notch ligands, respectively. Dashed arrows show transcriptional activation. at, atrium; lv, left ventricle.

Development (2018) 145, dev163378. doi:10.1242/dev.163378

effectors, the endocardium showed features of chamber tissue, and EMT did not occur (Fig. 6A,D). Ectopic *Bmp2* expression in the ventricles increased pSmad1/5 levels, resulting in transcriptional activation of Notch ligands, expansion of Notch pathway activity, and cooperation between the two pathways for EMT induction and valve specification in both AVC and chamber tissue (Fig. 6B,E).

MATERIALS AND METHODS

Mouse strains and genotyping

Animal studies were approved by the CNIC Animal Experimentation Ethics Committee and the Community of Madrid (Ref. PROEX 118/15). All animal procedures conformed to EU Directive 2010/63EU and Recommendation 2007/526/EC regarding the protection of animals used for experimental and other scientific purposes, enforced in Spanish law under Real Decreto 1201/2005. The following mouse strains were used: *Bmp2*^{GOF}, *Nkx2.5-Cre* (Stanley et al., 2002), cardiac *TnT-Cre* (Jiao et al., 2003), *Tie2-Cre* (Kisanuki et al., 2001) and *Mesp1-Cre* (Saga et al., 1999). To generate *Bmp2*^{GOF} mice, a cDNA encoding *Bmp2* was cloned into a modified version of the *pROSA26-1* plasmid, preceded by a loxP-flanked 'Neo^{R}-STOP' cassette and followed by an IRES-EGFP cassette. Gene targeting, performed in G4 embryonic stem cells, was confirmed by Southern blotting with 5′ and 3′ probes. Mice were generated by injection of targeted cells into B6CRL blastocysts to generate chimeras that were then analyzed for germline transmission. The selected animals were backcrossed to the C57BL/6 background. All reported controls are Cre driver heterozygotes.

Histology and *in situ* hybridization

H&E, Alcian Blue staining, X-gal staining and *in situ* hybridization on paraffin sections and in whole embryos were performed as described (de la Pompa et al., 1997). The primers used were: Smurf1 F, 5′-GGAAACCT-GTGGCTTTGCAG-3′; R, 5′-CCATCACACCTGCTTTGTGC-3′; Smurf2 F, 5′-CACGGTTGCTCCAGTTTGTG-3′; R, 5′-CCGACTGCTGGAGTTGT-CTT-3′. Details of the other probes used can be found in D'Amato et al. (2016), MacGrogan et al. (2016), Christoffels et al. (2000) and Bruneau et al. (2001).

Immunohistochemistry

Paraffin sections (7 µm thick) were incubated overnight with primary antibodies, followed by 1 h incubation with the appropriate secondary antibody conjugated to a fluorescent dye. Staining for N1ICD, Jag1 and phospho-Smad1/5 was performed using tyramide signal amplification (Del Monte et al., 2007). For same-species double staining (pSmad1/5 and N1ICD), two sequential assays were performed combining two unlabeled rabbit antibodies in separate detection sequences. Cross-reactions were prevented by extensive blocking with excess unconjugated Fab anti-rabbit IgG (1 h) and 5 min heating in citrate buffer between the two assays. Experiments omitting the first or second primary antibody were used routinely to control for unwanted background staining. Antibodies were used against the following targets: phospho-Smad1/5 (Cell Signaling, 9516, 1:100), Sox9 (Santa Cruz, sc-20095, 1:100), BrdU (AbCam, ab6326, 1:100), Isolectin GS-IB4-Alexa Fluor 647 (Molecular Probes, mp132450, 1:200), cleaved Notch1 (N1ICD, Cell Signaling, 4147, 1:100), α-smooth muscle actin-Cy3 (Sigma, C6198, 1:200) and Snail1 (1:50; Francí et al., 2006).

Quantification of incorporated BrdU and pSmad1/5 staining

Cell proliferation was analyzed at E9.5 after a 2 h BrdU pulse by detecting incorporated BrdU on paraffin sections. The number of positive nuclei, in both the myocardium (isolectin-B4-negative cells) and endocardium (isolectin-B4-positive cells), was divided by the total number of nuclei counted on four sections (at different levels) in three embryos per genotype. pSmad1/5-positive cells were counted similarly. Images were processed with ImageJ (image processing and analysis in Java). Data are presented as mean±s.d.

Quantification of histology sections

Measurements were performed with ImageJ on H&E-stained paraffin sections using morphological criteria. The length of the AVC was measured by drawing a line from the boundary between the atrium and AVC to the boundary between the ventricle and AVC (determined by the presence of trabeculae). The area occupied by the AVC was measured by delimiting the AVC using the aforementioned criteria, applying the 'area' tool and normalizing against the area of the heart at the four-chamber level. The length of the trabeculae and the distance between endocardium and myocardium were calculated by taking several measurements from the compact myocardium to either the tip of the trabeculae (six trabeculae per section when available) or the endocardium (six different areas throughout the ventricle). Three sections (at different levels) of four to seven embryos per genotype were measured (each data point represents an embryo). Data are presented as mean±s.d.

AVC and ventricular explant cultures on collagen gels

Explant cultures were performed as previously described (Runyan and Markwald, 1983; Luna-Zurita et al., 2010). For treatments with the γ-secretase inhibitor RO (Munch et al., 2013), collagen gels were pre-conditioned in explant medium containing 20 µM RO or vehicle (DMSO). The myocardium was removed from RO-treated explants for better *z*-axis visualization. Data are presented as mean±s.d.

Explant culture immunohistochemistry

Explants were fixed and stained with phalloidin-Alexa Fluor 488 (Invitrogen, A12379) and anti-α-smooth muscle actin-Cy3 (1:100; Sigma, C6198) to detect the actin cytoskeleton and mesenchymal cells, respectively. Explants were then mounted on excavated slides in Vectashield medium containing DAPI.

Explant culture quantification

The 3D TI of AVC and ventricular explants is the ratio of the number of cells invading the collagen gel to the total number of cells counted by DAPI staining, excluding the myocardium. The average distance and depth of invasion were measured manually in ImageJ on *x*-*y* and *x*-*z* axes images. Six independent measurements were performed on each explant. A total of 10-14 explants were examined per condition. Data are presented as mean±s.d.

Confocal imaging

Confocal images of stained explants and tissue sections were acquired with a Nikon A1R laser-scanning confocal microscope. Images of stained explants were collected as *z*-stacks. *z*-projections and lateral sections were assembled using ImageJ.

Cell culture

Immortalized MEVECs, derived from E10.5 ventricles, were cultured as described (D'Amato et al., 2016). MEVECs were co-cultured for 6 h with *GFP*-, *Jag1*- or *Dll4*-expressing OP9 cells at 80% confluence in DMEM supplemented with 10% fetal bovine serum (FBS) and antibiotics. Overnight serum-free incubation was followed by a 5-h treatment with 20 ng/ml human recombinant BMP2. All cells were then washed in cold PBS and harvested for either immunoprecipitation or RNA extraction. Alternatively, MEVECs were incubated overnight in serum-free medium and then treated for 5 h with BMP2, as previously described. Material was collected for ChIP assay, as described below. Bovine aortic endothelial cells (BAECs) were cultured on 0.1% gelatin-coated plates in complete DMEM supplemented with 10% FBS and antibiotics, and were used for luciferase assays at 95% confluence.

Quantitative RT-PCR

Total RNA from cells was extracted with Trizol (Invitrogen). cDNA was synthesized from 1 µg of total RNA using the SuperScript III First Strand kit (Invitrogen). qPCR was performed with the Power SYBR Green Master Mix (Applied Biosystems) and KiCqStart Primers (Sigma-Aldrich). Tissue samples from seven embryos of each genotype were pooled; three pools were used for the analysis. Data are presented as mean±s.d.

Genomic *Jag1* DNA fragments

The Evolutionary Conserved Region platform (ECR; http://ecrbrowser.dcode.org) was used to identify the mouse orthologs of the two previously identified

Development (2018) 145, dev163378. doi:10.1242/dev.163378

SMAD1-binding regions in the human *JAG1* locus, within the second intron and the promoter, approximately 520 bp upstream of the transcription start site (TSS) (Morikawa et al., 2011). Genomic DNA from E9.5 mouse embryos was used as a template to amplify 1162 bp (intronic) and 761 bp (promoter), containing the regions of interest (Fig. S9). The intronic product was cloned into the *Kpn*I/*Xho*I sites and the promoter product into the *Kpn*I/*Hind*III sites of the pGL3 luciferase plasmid. The primer sequences were: 5′-ATGCGGTACCCATCTGGCAGTAAGGTGGCT-3′ (intronic, forward, *Kpn*I site underlined), 5′-ATCGCTCGAGTGAACTGGACGGTTGTGCTT-3′ (intronic, reverse, *Xho*I site underlined), 5′-ATGCGGTACCAAGGAACCTGGAAGGACCGT-3′ (promoter, forward, *Kpn*I site underlined), and 5′-ATCGAAGCTTCCAGGAGTGTCGCTGCTAAT-3′ (promoter, reverse, *Hind*III site underlined).

Luciferase assay

BAECs were transiently transfected with the Notch reporter pGL3-10xCBF1-Luciferase (McKenzie et al., 2005) or the Bmp reporter pBRE-Luciferase (Korchynskyi and ten Dijke, 2002) or the mouse *Jag1* genomic luciferase constructs at a 5:1 ratio with pGL3-*Renilla* using Lipofectamine LTX (Life Technologies). Notch stimulation was achieved by transient co-transfection of a Myc-tagged N1ICD-expressing plasmid (N1ICDΔ^{OP}) (Milner et al., 1996) and Bmp stimulation by co-transfection of a pcDNA3 plasmid expressing constitutively active Alk3 (caAlk3) (ten Dijke et al., 1993), kindly provided by P. ten Dijke (Leiden University, The Netherlands). Fetal bovine serum was added to the medium 4 h after transfection, to a final concentration of 5%. After 20 h of incubation, luciferase activity was measured with the Dual Luciferase Assay System (Promega). The firefly/*Renilla* luciferase ratios are presented as mean±s.d. Experiments were performed at least three times, in quadruplicate for each experiment. Differences were considered statistically significant at $P<0.05$, as assessed by one-way ANOVA.

Chromatin immunoprecipitation

MEVECs (untreated and BMP2-treated) were fixed in 1% formaldehyde for 5 min at room temperature and quenched by glycine 125 mM for 5 min at room temperature. After three washes in cold PBS, cells were harvested and snap-frozen in liquid nitrogen. Briefly, pellets from 2×10^7 cells were re-suspended and incubated in 1 ml of Lysis Buffer 1 [50 mM HEPES-KOH (pH 7.5), 140 mM NaCl, 1 mM EDTA, 10% glycerol, 0.5% NP-40, 0.25% Triton X-100] and 1 ml of Lysis Buffer 2 (200 mM NaCl, 1 mM EDTA, 0.5 mM EGTA, 10 mM Tris pH 8) consecutively. The resulting pellet was re-suspended in Lysis Buffer 3 (1% NP-40, 0.5% sodium deoxycholate, 0.1% SDS, in 1×PBS) and chromatin was sheared by sonication using a Bioruptor ultrasonicator (Diagenode). Sheared chromatin was split and immunoprecipitated with 10 µl of anti-Smad1 (Cell Signaling, 6944) or rabbit IgG (Santa Cruz Biotechnology, sc-2027).

ChIP qPCR

Equal amounts of input and IgG/Smad1 immunoprecipitated DNA were used for qPCR analysis. The primer sequences were: 5′-GCACCATGAAGCTGGAAGAATCT-3′ (negative, forward), 5′-TACCCAAAGGAGCATAGCGTT-3′ (negative, reverse), 5′-TGGTCTAAATCGGGCCACTAAC-3′ (positive, Smad7, forward), 5′-AGCAGGGGGAAATCGGAAGAG-3′ (positive, Smad7, reverse), 5′-GCTGGGAGCTTCCTTTTCCT-3′ (Jag1 intronic, forward), 5′-ATGGCGGTTTGTTTGTGTCG-3′ (Jag1 intronic, reverse), 5′-CAGACTCTGCTGGGAACTTTG-3′ (Jag1 promoter, forward) and 5′-GGACATGGATTTGGGAAGG-3′ (Jag1 promoter, reverse). For data quantification, after normalizing to input, Smad1/IgG fold-enrichment was calculated. Differences were considered statistically significant at $P<0.05$, as assessed by one-way ANOVA for multiple comparisons. Data are represented as mean-fold enrichment±s.d. of at least three independent experiments.

Immunoprecipitation

Cells were harvested from 100 mm culture dishes in IONIC buffer (50 mM TrisHCl pH 8.0, 150 mM NaCl, 0.5% NP40, 0.5% sodium deoxycholate, 0.05% SDS) containing protease, phosphatase and proteasome inhibitors (MG-132). After crosslinking of the antibody of interest to Protein G Dynabeads (Thermo Fisher Scientific, 10003D) with dimethyl pimelimidate, the protein lysates were centrifuged and immunoprecipitated overnight at 4°C. The antibody-bound proteins were then eluted from the beads in 0.5 M glycine pH 2.5. Then, TrisHCl 1M (pH 8.8) was added at 10% of the sample volume to restore the pH. The antibodies used for immunoprecipitation were anti-c-Myc (5 µg; Invitrogen, 13-2500), anti-Notch1 (1:50; Cell Signaling, 3608) and anti-Smad1 (1:100; Cell Signaling, 6944). The Myc antibody was used for the detection and precipitation of the Myc-tagged form of N1ICD (N1ICDΔ^{OP}) (Milner et al., 1996).

Western blot

Three pools of six control and six *Bmp2*^{GOF}*;Nkx2.5-Cre* E9.5 hearts were lysed in RIPA buffer (TrisHCl 50 mM pH 8.0, NaCl 150 mM, NP40 1%, sodium deoxycholate 0.5%, SDS 0.1%) containing protease and phosphatase inhibitors at 4°C for 30 min. After centrifugation at 16000 ***g*** for 20 min at 4ºC, the supernatants were denatured with Laemmli buffer at 95°C for 5 min. Equal amounts of input (25 µg) and immunoprecipitated samples or 60 µg of cardiac lysates were separated by SDS-PAGE and transferred to PVDF membranes (Millipore) under standard conditions. Blots were probed with antibodies to phospho-Smad1/5 (1:1000; Cell Signaling, 9516), Notch1 (1:1000; Cell Signaling, 3608), c-Myc (1:2000; Invitrogen, 13-2500), PCNA (1:5000; BD Biosciences, 610665) and alpha-tubulin (1:5000; Sigma, T8203). Bound HRP-conjugated secondary antibodies were detected by ECL (GE Healthcare). Band intensities were quantified by densitometric analysis using ImageJ software.

RNA sequencing

Total RNA was isolated at E9.5 from whole hearts of control and *Bmp2*^{GOF}*;Nkx2.5-Cre* embryos (four pools of six hearts per genotype, 24 embryos in total per genotype) using the Arcturus PicoPure RNA isolation kit (AB, 12204). The RNA-seq was performed in the CNIC Genomics Unit: 200 ng of RNA were used to generate barcoded RNA-seq libraries using the NEBNext Ultra RNA Library preparation kit (New England Biolabs). Briefly, polyA+ RNA was purified using poly-T oligo-attached magnetic beads followed by fragmentation and then first and second cDNA strand synthesis. Next, cDNA 3′ ends were adenylated and the adapters were ligated, followed by PCR library amplification. Finally, the size of the libraries was checked using the Agilent 2100 Bioanalyzer DNA 1000 chip and their concentration was determined using the Qubit fluorometer (Life Technologies). Libraries were sequenced on a HiSeq2500 (Illumina) to generate 60-bp single reads. FastQ files for each sample were obtained using CASAVA v1.8 software (Illumina). Sequencing reads were preprocessed by means of a pipeline that used FastQC (www.bioinformatics.babraham.ac.uk/projects/fastqc/) to assess read quality, and Cutadapt 1.7.1 to trim sequencing reads, eliminating Illumina adaptor remains and discarding reads that were shorter than 30 bp. The resulting reads were mapped against the mouse transcriptome (GRCm38, release 76; aug2014 archive) and quantified using RSEM v1.2.20 (Li and Dewey, 2011). Data were then processed with a differential expression analysis pipeline that used the Bioconductor package limma (Ritchie et al., 2015) for normalization and differential expression testing.

Interactome prediction of Bmp2-dependent genes

The 2000 DEGs with the lowest *P* values identified by our RNA-seq were used as input node data into the STRING 10.0 (http://string-db.org/) database (Szklarczyk et al., 2015). To obtain more stringent interactions, the Textmining interaction source was excluded, and the minimum required interaction score considered was 0.7 (high confidence). Resultant networks were then replotted using Cytoscape 3.4.0 (www.cytoscape.org/) (Shannon et al., 2003) with the force-directed layout setting. Hubs were defined as the upregulated nodes with the most direct neighbors of the 2000 DEGs.

Gene ontology and KEGG pathway enrichment analysis

GO and KEGG Pathway enrichment analyses of DEGs were performed using GO-Elite (www.genmapp.org/go_elite/; 1.2.5, EnsMart77Plus database version) (Zambon et al., 2012). For the analysis of the RNA-seq results, we used as background the 13,637 genes considered to be expressed. For the comparison between the RNA-seq from this report and RNA-seq

Development (2018) 145, dev163378. doi:10.1242/dev.163378

from Prados et al. (2018), we used as background the 12,435 genes considered to be expressed in both data sets. *z*-score of the terms in the different categories (Biological process, Cellular component, Molecular function and KEGG pathways) were represented in heatmaps using GraphPad Prism 7.

Statistical analysis

Statistical significance was assessed using Student's *t*-test, unless otherwise stated (*P<0.05, **P<0.01, ***P<0.001).

Acknowledgements

We thank V. Bou and A. Galicia for animal husbandry, S. Bartlett (CNIC) for English editing, and Fátima Sanchez for statistical support. We also thank the Genomics, Bioinformatics, Pluripotent Cell Technology and Transgenesis units at the CNIC.

Competing interests

The authors declare no competing or financial interests.

Author contributions

Conceptualization: J.L.d.l.P.; Methodology: J.L.d.l.P., B.P., T.P.; Validation: J.L.d.l.P. Formal analysis: T.P., L.L.-Z.; Investigation: T.P., B.P., L.L.-Z.; Resources: J.L.d.l.P., S.Z.; Data curation: J.L.d.l.P.; Writing - original draft: T.P.; Writing - review & editing: J.L.d.l.P.; Visualization: T.P., L.L.-Z., J.L.d.l.P.; Supervision: J.L.d.l.P., S.Z.; Project administration: J.L.d.l.P.; Funding acquisition: J.L.d.l.P., S.Z.

Funding

This study was funded by grants SAF2016-78370-R and CB16/11/00399 (Ciber Cardiovascular), RD12/0019/0003 and RD16/0011/0021 (Red de Terapia Celular, TERCEL) from the Spanish Ministry of Science, Innovation and Universities [Ministerio de Ciencia, Industria y Universidades (MCIU)], and by grants from the Fundación BBVA (BIO14_298) and Fundació la Marató de TV3 (20153431) to J.L.d.l.P. T.P. was supported by a postdoctoral contract associated with grant BIO14_298, B.P. by a postdoctoral contract associated with grant RD12/0019/0003, and L.L.-Z. by a Centro Nacional de Investigaciones Cardiovasculares Carlos III (CNIC) IPP FP7 Marie Curie Programme (PCFUND-201-600396) postdoctoral contract and a Ramón y Cajal postdoctoral contract (RYC-2016-20917). The CNIC is supported by the Ministerio de Ciencia, Industria y Universidades and the Pro CNIC Foundation, and is a Severo Ochoa Center of Excellence (SEV-2015-0505). S.Z.'s laboratory was supported by the Fondation pour la Recherche Médicale (DPC20111123002).

Data availability

RNA-seq data have been deposited in the NCBI Gene Expression Omnibus database under accession number GSE104670.

Supplementary information

Supplementary information available online at
http://dev.biologists.org/lookup/doi/10.1242/dev.163378.supplemental

References

Blokzijl, A., Dahlqvist, C., Reissmann, E., Falk, A., Moliner, A., Lendahl, U. and Ibáñez, C. F. (2003). Cross-talk between the Notch and TGF-beta signaling pathways mediated by interaction of the Notch intracellular domain with Smad3. *J. Cell Biol.* **163**, 723-728.

Bonilla-Claudio, M., Wang, J., Bai, Y., Klysik, E., Selever, J. and Martin, J. F. (2012). Bmp signaling regulates a dose-dependent transcriptional program to control facial skeletal development. *Development* **139**, 709-719.

Bruneau, B. G., Bao, Z.-Z., Fatkin, D., Xavier-Neto, J., Georgakopoulos, D., Maguire, C. T., Berul, C. I., Kass, D. A., Kuroski-de Bold, M. L., de Bold, A. J. et al. (2001). Cardiomyopathy in Irx4-deficient mice is preceded by abnormal ventricular gene expression. *Mol. Cell. Biol.* **21**, 1730-1736.

Chandhoke, A. S., Karve, K., Dadakhujaev, S., Netherton, S., Deng, L. and Bonni, S. (2016). The ubiquitin ligase Smurf2 suppresses TGFbeta-induced epithelial-mesenchymal transition in a sumoylation-regulated manner. *Cell Death Differ.* **23**, 876-888.

Christoffels, V. M., Keijser, A. G. M., Houweling, A. C., Clout, D. E. W. and Moorman, A. F. M. (2000). Patterning the embryonic heart: identification of five mouse Iroquois homeobox genes in the developing heart. *Dev. Biol.* **224**, 263-274.

Christoffels, V. M., Hoogaars, W. M. H., Tessari, A., Clout, D. E. W., Moorman, A. F. M. and Campione, M. (2004). T-box transcription factor Tbx2 represses differentiation and formation of the cardiac chambers. *Dev. Dyn.* **229**, 763-770.

D'Amato, G., Luxán, G., del Monte-Nieto, G., Martínez-Poveda, B., Torroja, C., Walter, W., Bochter, M. S., Benedito, R., Cole, S., Martinez, F. et al. (2016). Sequential Notch activation regulates ventricular chamber development. *Nat. Cell Biol.* **18**, 7-20.

de Boer, B. A., van den Berg, G., de Boer, P. A. J., Moorman, A. F. M. and Ruijter, J. M. (2012). Growth of the developing mouse heart: an interactive qualitative and quantitative 3D atlas. *Dev. Biol.* **368**, 203-213.

de la Pompa, J. L., Wakeham, A., Correia, K. M., Samper, E., Brown, S., Aguilera, R. J., Nakano, T., Honjo, T., Mak, T. W., Rossant, J. et al. (1997). Conservation of the Notch signalling pathway in mammalian neurogenesis. *Development* **124**, 1139-1148.

Del Monte, G., Grego-Bessa, J., González-Rajal, A., Bolós, V. and De La Pompa, J. L. (2007). Monitoring Notch1 activity in development: evidence for a feedback regulatory loop. *Dev. Dyn.* **236**, 2594-2614.

Eisenberg, L. M. and Markwald, R. R. (1995). Molecular regulation of atrioventricular valvuloseptal morphogenesis. *Circ. Res.* **77**, 1-6.

Francí, C., Takkunen, M., Dave, N., Alameda, F., Gómez, S., Rodríguez, R., Escrivà, M., Montserrat-Sentís, B., Baró, T., Garrido, M. et al. (2006). Expression of Snail protein in tumor-stroma interface. *Oncogene* **25**, 5134-5144.

Grego-Bessa, J., Luna-Zurita, L., del Monte, G., Bolós, V., Melgar, P., Arandilla, A., Garratt, A. N., Zang, H., Mukouyama, Y.-S., Chen, H. et al. (2007). Notch signaling is essential for ventricular chamber development. *Dev. Cell* **12**, 415-429.

Habets, P. E. M. H., Moorman, A. F. M., Clout, D. E. W., van Roon, M. A., Lingbeek, M., van Lohuizen, M., Campione, M. and Christoffels, V. M. (2002). Cooperative action of Tbx2 and Nkx2.5 inhibits ANF expression in the atrioventricular canal: implications for cardiac chamber formation. *Genes Dev.* **16**, 1234-1246.

Harrelson, Z., Kelly, R. G., Goldin, S. N., Gibson-Brown, J. J., Bollag, R. J., Silver, L. M. and Papaioannou, V. E. (2004). Tbx2 is essential for patterning the atrioventricular canal and for morphogenesis of the outflow tract during heart development. *Development* **131**, 5041-5052.

Hoogaars, W. M. H., Tessari, A., Moorman, A. F. M., de Boer, P. A. J., Hagoort, J., Soufan, A. T., Campione, M. and Christoffels, V. M. (2004). The transcriptional repressor Tbx3 delineates the developing central conduction system of the heart. *Cardiovasc. Res.* **62**, 489-499.

Hoogaars, W. M. H., Engel, A., Brons, J. F., Verkerk, A. O., de Lange, F. J., Wong, L. Y. E., Bakker, M. L., Clout, D. E., Wakker, V., Barnett, P. et al. (2007). Tbx3 controls the sinoatrial node gene program and imposes pacemaker function on the atria. *Genes Dev.* **21**, 1098-1112.

Itoh, F., Itoh, S., Goumans, M.-J., Valdimarsdottir, G., Iso, T., Dotto, G. P., Hamamori, Y., Kedes, L., Kato, M. and ten Dijke, P. (2004). Synergy and antagonism between Notch and BMP receptor signaling pathways in endothelial cells. *EMBO J.* **23**, 541-551.

Jiao, K., Kulessa, H., Tompkins, K., Zhou, Y., Batts, L., Baldwin, H. S. and Hogan, B. L. M. (2003). An essential role of Bmp4 in the atrioventricular septation of the mouse heart. *Genes Dev.* **17**, 2362-2367.

Kisanuki, Y. Y., Hammer, R. E., Miyazaki, J., Williams, S. C., Richardson, J. A. and Yanagisawa, M. (2001). Tie2-Cre transgenic mice: a new model for endothelial cell-lineage analysis in vivo. *Dev. Biol.* **230**, 230-242.

Korchynskyi, O. and ten Dijke, P. (2002). Identification and functional characterization of distinct critically important bone morphogenetic protein-specific response elements in the Id1 promoter. *J. Biol. Chem.* **277**, 4883-4891.

Li, B. and Dewey, C. N. (2011). RSEM: accurate transcript quantification from RNA-Seq data with or without a reference genome. *BMC Bioinformatics* **12**, 323.

Luna-Zurita, L., Prados, B., Grego-Bessa, J., Luxán, G., del Monte, G., Benguría, A., Adams, R. H., Pérez-Pomares, J. M. and de la Pompa, J. L. (2010). Integration of a Notch-dependent mesenchymal gene program and Bmp2-driven cell invasiveness regulates murine cardiac valve formation. *J. Clin. Invest.* **120**, 3493-3507.

Ma, L., Lu, M.-F., Schwartz, R. J. and Martin, J. F. (2005). Bmp2 is essential for cardiac cushion epithelial-mesenchymal transition and myocardial patterning. *Development* **132**, 5601-5611.

MacGrogan, D., D'Amato, G., Travisano, S., Martinez-Poveda, B., Luxán, G., del Monte-Nieto, G., Papoutsi, T., Sbroggio, M., Bou, V., Gomez-del Arco, P. et al. (2016). Sequential ligand-dependent Notch signaling activation regulates valve primordium formation and morphogenesis novelty and significance. *Circ. Res.* **118**, 1480-1497.

McKenzie, G. J., Stevenson, P., Ward, G., Papadia, S., Bading, H., Chawla, S., Privalsky, M. and Hardingham, G. E. (2005). Nuclear Ca2+ and CaM kinase IV specify hormonal- and Notch-responsiveness. *J. Neurochem.* **93**, 171-185.

Milner, L. A., Bigas, A., Kopan, R., Brashem-Stein, C., Bernstein, I. D. and Martin, D. I. K. (1996). Inhibition of granulocytic differentiation by mNotch1. *Proc. Natl. Acad. Sci. USA* **93**, 13014-13019.

Moorman, A., Webb, S., Brown, N. A., Lamers, W. and Anderson, R. H. (2003). Development of the heart: (1) formation of the cardiac chambers and arterial trunks. *Heart* **89**, 806-814.

Morikawa, M., Koinuma, D., Tsutsumi, S., Vasilaki, E., Kanki, Y., Heldin, C.-H., Aburatani, H. and Miyazono, K. (2011). ChIP-seq reveals cell type-specific binding patterns of BMP-specific Smads and a novel binding motif. *Nucleic Acids Res.* **39**, 8712-8727.

Moya, I. M., Umans, L., Maas, E., Pereira, P. N. G., Beets, K., Francis, A., Sents, W., Robertson, E. J., Mummery, C. L., Huylebroeck, D. et al. (2012). Stalk cell

phenotype depends on integration of Notch and Smad1/5 signaling cascades. *Dev. Cell* **22**, 501-514.

Munch, J., Gonzalez-Rajal, A. and de la Pompa, J. L. (2013). Notch regulates blastema proliferation and prevents differentiation during adult zebrafish fin regeneration. *Development* **140**, 1402-1411.

Ozdamar, B., Bose, R., Barrios-Rodiles, M., Wang, H. R., Zhang, Y. and Wrana, J. L. (2005). Regulation of the polarity protein Par6 by TGFbeta receptors controls epithelial cell plasticity. *Science* **307**, 1603-1609.

Prados, B., Gómez-Apiñániz, P., Papoutsi, T., Luxán, G., Zaffran, S., Pérez-Pomares, J. M. and de la Pompa, J. L. (2018). Myocardial Bmp2 gain causes ectopic EMT and promotes cardiomyocyte proliferation and immaturity. *Cell Death Dis.* **9**, 399.

Ritchie, M. E., Phipson, B., Wu, D., Hu, Y., Law, C. W., Shi, W. and Smyth, G. K. (2015). limma powers differential expression analyses for RNA-sequencing and microarray studies. *Nucleic Acids Res.* **43**, e47.

Rivera-Feliciano, J. and Tabin, C. J. (2006). Bmp2 instructs cardiac progenitors to form the heart-valve-inducing field. *Dev. Biol.* **295**, 580-588.

Runyan, R. B. and Markwald, R. R. (1983). Invasion of mesenchyme into three-dimensional collagen gels: a regional and temporal analysis of interaction in embryonic heart tissue. *Dev. Biol.* **95**, 108-114.

Saga, Y., Miyagawa-Tomita, S., Takagi, A., Kitajima, S., Miyazaki, J. and Inoue, T. (1999). MesP1 is expressed in the heart precursor cells and required for the formation of a single heart tube. *Development* **126**, 3437-3447.

Sedmera, D., Pexieder, T., Vuillemin, M., Thompson, R. P. and Anderson, R. H. (2000). Developmental patterning of the myocardium. *Anat. Rec.* **258**, 319-337.

Shannon, P., Markiel, A., Ozier, O., Baliga, N. S., Wang, J. T., Ramage, D., Amin, N., Schwikowski, B. and Ideker, T. (2003). Cytoscape: a software environment for integrated models of biomolecular interaction networks. *Genome Res.* **13**, 2498-2504.

Shirai, M., Imanaka-Yoshida, K., Schneider, M. D., Schwartz, R. J. and Morisaki, T. (2009). T-box 2, a mediator of Bmp-Smad signaling, induced hyaluronan synthase 2 and Tgfbeta2 expression and endocardial cushion formation. *Proc. Natl. Acad. Sci. USA* **106**, 18604-18609.

Singh, R. and Kispert, A. (2010). Tbx20, Smads, and the atrioventricular canal. *Trends Cardiovasc. Med.* **20**, 109-114.

Singh, M. K., Christoffels, V. M., Dias, J. M., Trowe, M.-O., Petry, M., Schuster-Gossler, K., Bürger, A., Ericson, J. and Kispert, A. (2005). Tbx20 is essential for cardiac chamber differentiation and repression of Tbx2. *Development* **132**, 2697-2707.

Singh, R., Hoogaars, W. M., Barnett, P., Grieskamp, T., Rana, M. S., Buermans, H., Farin, H. F., Petry, M., Heallen, T., Martin, J. F. et al. (2012). Tbx2 and Tbx3 induce atrioventricular myocardial development and endocardial cushion formation. *Cell. Mol. Life Sci.* **69**, 1377-1389.

Stanley, E. G., Biben, C., Elefanty, A., Barnett, L., Koentgen, F., Robb, L. and Harvey, R. P. (2002). Efficient Cre-mediated deletion in cardiac progenitor cells conferred by a 3'UTR-ires-Cre allele of the homeobox gene Nkx2-5. *Int. J. Dev. Biol.* **46**, 431-439.

Sugi, Y., Yamamura, H., Okagawa, H. and Markwald, R. R. (2004). Bone morphogenetic protein-2 can mediate myocardial regulation of atrioventricular cushion mesenchymal cell formation in mice. *Dev. Biol.* **269**, 505-518.

Szklarczyk, D., Franceschini, A., Wyder, S., Forslund, K., Heller, D., Huerta-Cepas, J., Simonovic, M., Roth, A., Santos, A., Tsafou, K. P. et al. (2015). STRING v10: protein-protein interaction networks, integrated over the tree of life. *Nucleic Acids Res.* **43**, D447-D452.

Takizawa, T., Ochiai, W., Nakashima, K. and Taga, T. (2003). Enhanced gene activation by Notch and BMP signaling cross-talk. *Nucleic Acids Res.* **31**, 5723-5731.

ten Dijke, P., Ichijo, H., Franzen, P., Schulz, P., Saras, J., Toyoshima, H., Heldin, C. H. and Miyazono, K. (1993). Activin receptor-like kinases: a novel subclass of cell-surface receptors with predicted serine/threonine kinase activity. *Oncogene* **8**, 2879-2887.

Timmerman, L. A., Grego-Bessa, J., Raya, A., Bertran, E., Perez-Pomares, J. M., Diez, J., Aranda, S., Palomo, S., McCormick, F., Izpisua-Belmonte, J. C. et al. (2004). Notch promotes epithelial-mesenchymal transition during cardiac development and oncogenic transformation. *Genes Dev.* **18**, 99-115.

Townsend, T. A., Wrana, J. L., Davis, G. E. and Barnett, J. V. (2008). Transforming growth factor-beta-stimulated endocardial cell transformation is dependent on Par6c regulation of RhoA. *J. Biol. Chem.* **283**, 13834-13841.

Yamada, M., Revelli, J.-P., Eichele, G., Barron, M. and Schwartz, R. J. (2000). Expression of chick Tbx-2, Tbx-3, and Tbx-5 genes during early heart development: evidence for BMP2 induction of Tbx2. *Dev. Biol.* **228**, 95-105.

Zambon, A. C., Gaj, S., Ho, I., Hanspers, K., Vranizan, K., Evelo, C. T., Conklin, B. R., Pico, A. R. and Salomonis, N. (2012). GO-Elite: a flexible solution for pathway and ontology over-representation. *Bioinformatics* **28**, 2209-2210.

Zhang, Y., Chang, C., Gehling, D. J., Hemmati-Brivanlou, A. and Derynck, R. (2001). Regulation of Smad degradation and activity by Smurf2, an E3 ubiquitin ligase. *Proc. Natl. Acad. Sci. USA* **98**, 974-979.